PCCP

The role of halogen bonding in metal free phosphors

Journal:	*Physical Chemistry Chemical Physics*
Manuscript ID	CP-ART-03-2021-001325.R1
Article Type:	Paper
Date Submitted by the Author:	09-Sep-2021

Complete List of Authors:	Ansari, Ramin; University of Michigan, Department of Chemical Engineering Hashemi, Daniel; Toyota Research Institute North America, Kieffer, John; University of Michigan, Materials Science and Engineering;

PAPER

The role of halogen bonding in metal free phosphors

Ramin Ansari,[a] Daniel Hashemi [b] and John Kieffer *[b]

Received 00th January 20xx,
Accepted 00th January 20xx

DOI: 10.1039/x0xx00000x

The enhanced spin-orbit coupling necessary for phosphorescence is thought to be due to the halogen bonding that is present in the all-organic crystalline systems.[1] To elucidate the underlying mechanism, the electronic and optical properties of purely organic phosphor candidates are investigated using density functional theory calculations. The unit cell structure of a known organic phosphor containing bromine is used to validate the accuracy of the computational methodology. Compared to experiments, the calculated lattice constants deviate by less than 1 percent for each lattice constant. The same computational approach is then used to predict the lattice constants for molecular analogs containing fluorine, chlorine, and iodine. Electronic structure and photonic properties of the predicted crystals are computed. Finally, the presence of halogen bonding is corroborated, with fluorine forming the weakest and iodine the strongest halogen bonding interactions. Our findings demonstrate how computational methods can be effectively used for the predictive design of organic materials in lighting devices.

1 INTRODUCTION

Organic light emitting diodes (OLEDs) based on transition metal complexes have been widely investigated over recent decades for their display and solid-state lighting applications.[2] Increasing attention is devoted to phosphorescence materials because they can theoretically achieve threefold higher internal quantum efficiency than fluorescent alternatives, by harvesting triplet excitons through intersystem crossing (ISC).[3–6] Most candidates for efficient phosphorescence are based on heavy element complexes because the presence of a heavy atom enhances spin–orbit coupling (SOC) interactions,[7] which, in turn, augment the rate of the spin forbidden process. Although organometallic materials have high quantum efficiency, they require expensive and rare elements such as iridium[8] and platinum.[9] Organometallic materials also exhibit short operating lifetimes due to the degradation of weak and unstable metal-ligand bonds.[10]

Unlike organometallics, purely organic materials are less costly, lighter, readily functionalized, and easily processed. Until now, only a few examples of purely organic molecules with high phosphorescence quantum yield have been reported.[11] This scarcity is related to the fact that purely organic phosphors often exhibit long-lived triplet states that are easily dissipated by vibrational effects before emissive decay can take place. To be competitive with organometallic OLEDs, in purely organic materials one must (1) suppress vibrations that could cause non–radiative decays and (2) elevate intersystem crossing rates by increasing spin–orbit coupling interactions.

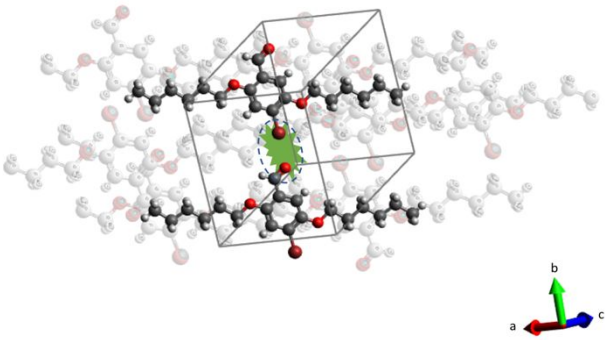

Figure 1 *The unit cell structure of the Br6A crystal.* The a lattice constant is along the x axis, the b lattice constant is along the y axis, and the c lattice constant is along the z axis.

To suppress vibrational relaxation of the triplet manifold, several approaches have been pursued. In 2011, Bolton et al.[1] reported enhanced room–temperature phosphorescence (RTP) from pure organic luminogens utilizing mixed crystals and halogen bonding. They designed chromophores that contain triplet-producing aromatic aldehyde and triplet-promoting bromine, and diluted them into the crystal of a bi-halogenated non-carbonyl analogue. One of the crystals they made is 2,5-dihexyloxy-4-bromobenzaldehyde (Fig. 1). 2,5-dihexyloxy-1,4-dibromobenzene (Br6) is a bi-halogenated analogue to Br6A. Br6 is the same as Br6A, but with a second bromine in place of its aldehyde. The resulting mixed crystals exhibit green phosphorescence with a much higher quantum yield compared to pure Br6A crystals. The ambient phosphorescence quantum yield for the resulting crystal reached 55%. Using this finding, they designed a series of

[a] Department of Chemical Engineering, University of Michigan, Ann Arbor, MI, 48109, USA.
[b] Department of Material Science and Engineering, University of Michigan, Ann Arbor, MI, 48109, USA. E-mail: kieffer@umich.edu

purely organic phosphors that emit blue, green, yellow and orange light. Follow-up studies by Lee et al.[12] explored embedding Br6A molecules into a glassy PMMA polymer film, which exhibits a bright 7.5% phosphorescence quantum yield due to strong halogen bonding between the bromine of Br6A molecules and the oxygen of PMMA polymer. Kwon et al.[13] designed a purely organic RTP system with an amorphous polymer matrix by exploiting strong noncovalent interactions such as hydrogen and halogen bonds, which effectively suppressed vibrational triplet decay and achieved a high phosphorescence quantum yield of 24%.

Furthermore, in 2013, Bergamini et al.[14] reported outstanding phosphorescence emission in some environments that impart rigidity. While no phosphorescence is recorded in solution at room temperature, the reported organic molecule shows a very bright phosphorescence in the solid state and at low temperature. In another work, Gao et al.[15–17] developed phosphorescence co-crystals based on halogen and hydrogen bonding. This peculiar behavior of phosphorescence emission in rigid environment is mainly attributed to the suppression of conformational mobility and bond rotation. However, it is unclear to what extent the halogen bonding contributes to efficient room temperature phosphorescence and how different halides affect the emission properties. Therefore, determining their relative influences provides better guidance for future metal-free organic phosphor development.

To promote ISC rates, a common molecular design for metal-free phosphors involves addition of a heavy atom to enhance the SOC interactions, which is either part of,[18, 19] or external to[20–22] the excited molecule. The enhanced SOC interactions promotes spin-forbidden processes including singlet to triplet ISC and radiative decay from the triplet to the singlet ground state. Halides, mostly bromine, have been widely used for the heavy atom effect in metal-free organic phosphors. The heavy atom effect is not the only factor that promotes ISC rates. The presence of aromatic carbonyl groups can also enhance the ISC process. The generation of the $n\pi^*$ state in aromatic carbonyls enhances ISC rates from an $n\pi^*$ singlet state to a $\pi\pi^*$ triplet state, or vice versa, based on the El-Sayed's rule.[23, 24] Furthermore, a small energy gap between first singlet state and the nearest triplet state also enhances ISC process.

In this paper, we computationally corroborate the existence of halogen bonding between the halogen and the carbonyl oxygen atoms of adjacent Br6A and other derivatives of this molecule. Strong halogen bonding in Br6A and its derivatives strongly suppresses vibrational dissipation and enables RTP with high quantum yields. This peculiar behavior is attributed to the restriction of bond rotation and conformational mobility of the molecule, which slows down the non-radiative deactivation processes of the phosphorescent excited state. The underlying mechanism of purely organic phosphor candidates is examined by means of a detailed computational study based on density functional theory (DFT) and time dependant DFT (TD-DFT) calculations, revealing the role of halogen bonding. Halogen substituted derivatives of Br6A as well as different Br6A conformations are investigated. The calculated density of states (DOS) is used to substantiate the halogen bonding interaction. This paper is organized as follows: section 2 describes the details of our DFT calculations; in section 3 the results are discussed; a conclusion and summary are given in section 4.

2 METHODOLOGIES

Four different Br6A systems are studied: isolated molecules, dimers, chains formed along the y-axis, which coincides with the halogen bond direction, and three-dimensional crystals. Isolated molecules are compared with dimers and chains in order to investigate the halogen bonding effect. All calculations are performed using plane-wave DFT as implemented in the Vienna ab-initio simulation package (VASP).[25, 26] The exchange-correlation energy and potential are described by Perdew, Burke and Ernzerhof (PBE) potentials.[27] The electron-ion interaction is described by the projector-augmented wave (PAW) scheme,[28, 29] and the electronic wave functions are expanded by plane waves up to a kinetic energy of 500 eV. The Brillouin zones are sampled using a $2 \times 2 \times 2$ Monkhorst-Pack mesh for the crystal case[30] and Gamma point for the isolated and dimer cases, since in this case there is no interaction between neighbor cells. The convergence of the calculated properties with respect to the number of k points and supercell size is ascertained. The many body dispersion method of Tkatchenko et al.[31] is used to account for van der Waals interactions. The spin-orbit coupling (SOC) was used within the noncollinear approach as implemented in VASP (see Ref. [32]).

The calculations have been carried out with and without taking the van der Waals interactions, spin polarization, and SOC interactions into account. Consequently, the relative weight of each interaction and its compounding effect in the overall behavior has been established. The experimental XRD data is only available for Br6A crystal.[1] However, for the other halogenated versions of this molecule (aka F6A, Cl6A and I6A), no experimental data is available. The electronic configurations of the halogens are similar; only their size and electronegativity are different. They do not create any additional dangling bonds nor missing bonds when substituted. Therefore, it is to be expected that with only one atom exchanged, the halogen, F6A, Cl6A, and I6A have unit cell structures similar to that of Br6A, and that the most significant changes are manifest in the lattice constants. Hence, using the atomic positions and orientations of Br6A as the starting coordinates for the new molecules, stable crystalline structures are derived based on accurate total energy minimization. The lattice constants for each compound can be determined by varying them independently along all 3 dimensions, and identifying the combination of *a*, *b*, and *c* values that result in the lowest energy. To validate this approach, we submit a slightly perturbed Br6A configuration to the minimization procedure. The experimental and calculated lattice constants are summarized in Table 1. Optimized lattice parameters of Br6A are found to be 9.51 Å, 9.64 Å and 10.85 Å, while the corresponding experimental

values are 9.51 Å, 9.69 Å and 10.95 Å, respectively. The lattice mismatch between the two is less than 1 percent for any lattice constant. After judiciously calculating the lattice constants for the other halogenated version of this molecule, we have analyzed the halogen bond formation of the X6A (X=F, Cl, Br, and I) molecules using the density of states (DOS), the real space charge density and the crystal orbital Hamilton population (COHP) analysis, which can provide important information about the local chemistry of the species.

The TD-DFT calculations were performed using Gaussian 16[33] for the molecular dimers. We used the B3LYP functional with the 6-31G(d,p) basis set, except that for Iodine atom we used the 3-21G basis set. Optimization of the ground state geometries is followed by an analysis of normal modes of atomic motion to confirm the stability of the optimized structures. The TD-DFT calculations are then carried out to study the nature of the low-lying excited states. Furthermore, the natural bond orbital (NBO) analysis is performed on molecular dimers in order to calculate the second-order E(2) interaction energies.

3 RESULTS AND DISCUSSION

Single-crystal X-ray diffraction (XRD) data for Br6A molecules indicates close proximity between the carbonyl oxygen and the bromine of the neighboring molecule. The measured value of 2.86 Å for the bromine–oxygen halogen bond length is among the shortest halogen bonds reported[34] and suggests definite electronic interaction between the two atoms. Moreover, phosphorescence from Br6A crystals is strong, but cannot be detected when Br6A is in solution. These experimental findings strongly suggest that halogen bonding is the prevalent reason for the remarkably efficient phosphorescence of Br6A. A halogen bond occurs when there is a net attractive interaction between an electrophilic region associated with a halogen atom in a molecular entity and a nucleophilic region in another, or the same molecular entity.[35] To investigate the existence of halogen bonding, DFT calculations are performed for Br6A dimers in which the spacing between the Br atom of one of the molecules and the aldehyde group of the other, i.e., the two moieties expected to form the halogen bond, is systematically varied. When simulations are carried out without accounting for van der Waals interactions, the minimum energy of the system occurs at a halogen bond length of 3.025 Å. By contrast, when including van der Waals interactions the molecules of the dimer approach closer to each other and the equilibrium halogen bond length drops to 2.976 Å. Since our system is not spin polarized, taking spin polarization into account has no effect on the halogen bond length. However, accounting for SOC interactions shortens to the halogen bond length to 2.936 Å. This trend highlights the interaction between the carbonyl oxygen and the bromine of the neighboring molecule. Moreover, performing the same calculations for a chain of Br6A molecules shows the same decreasing trend and clearly reveals the energy-lowering electronic interaction between the two atoms (Fig. 1).

Table 1 Calculated and experimental lattice constants for F6A, Cl6A, Br6A, and I6A

Lattice Constants	F6A[1]	Cl6A[1]	Br6A[1]	Br6A[2] (error)	I6A[1]
a	9.51 Å	9.51 Å	9.51 Å	9.51 Å (0%)	9.51 Å
b	9.49 Å	9.59 Å	9.69 Å	9.64 Å (0.52%)	9.79 Å
c	10.95 Å	10.95 Å	10.95 Å	10.85 Å (0.91%)	11.05 Å

[1] Calculated lattice constants
[2] Experimental lattice constants

The unit cell structure of the Br6A crystal, as derived from experimental XRD data,[1] is shown in Fig. 1. The structures of the other derivatives of this molecule, F6A, Cl6A and I6A, obtained using the approach described above, are geometrically similar, except for the differences in the unit cell parameters, which are reported in table 1.

All four halogen species are capable of acting as halogen bond donors and follow a general trend in terms of bond strength: F < Cl < Br < I, with iodine normally forming the strongest interactions.[36] When the halogen is bonded to an electron-withdrawing moiety, like phenyl, it is more likely to form stronger halogen bonds.[37] According to our calculations, the halogen bond distance in X6A molecules is 3.15 Å, 2.86 Å, 2.81 Å and 2.77 Å for X=F, Cl, Br and I, respectively, which follows the same trend as in the literature, and indicates that iodine forms the strongest and fluorine the weakest interaction. We have also calculated the formation energy of the halogen bonds. The formation energy is the amount of energy released upon the formation of a bond. Therefore, bond formation is always an exothermic process. As it can be seen from table 2, the bond formation energy for Cl, Br, and I are exothermic, which suggests formation of a strong halogen bond. In these molecules halogen and oxygen are located in close proximity, closer than the sum of the van der Waals radii (Table 2). These anomalously short intermolecular distances are among the strongest halogen bonds ever reported.

The standard procedure of handling halogen interactions is using sigma-hole and lone-pair to sigma* interactions.[38] Therefore, We have carried out a natural bond order B3LYP analysis of the molecular dimers. As can be seen in table 2 (NBO charge on halogen), our results show the presence of a positive electrostatic region on the outermost portion of the halogen's surface known as a σ-hole[38] for the Cl, Br and I derivatives. However, fluorine has a negative electronic charge on the outermost portion of its surface, which

Table 2 Calculated properties of halogen bond interaction for F6A, Cl6A, Br6A, and I6A

Crystal	F6A	Cl6A	Br6A	I6A
Halogen Bond Length (Å)	3.15	2.86	2.81	2.77
Sum of the van der Waals radius of oxygen and halogen (Å)	2.75	3.20	3.35	3.55
NBO charge on halogen	-0.339	+0.049	+0.103	+0.202
Formation energy of the halogen bond (eV)	+0.0225	-0.0612	-0.1097	-0.1773
Second-order E(2) interaction energy (kcal/mol)	0.06	2.13	4.39	10.12

substantiates the positive value of the halogen bond formation energy. These findings indicate that the interaction between F and the neighboring oxygen is repulsive.

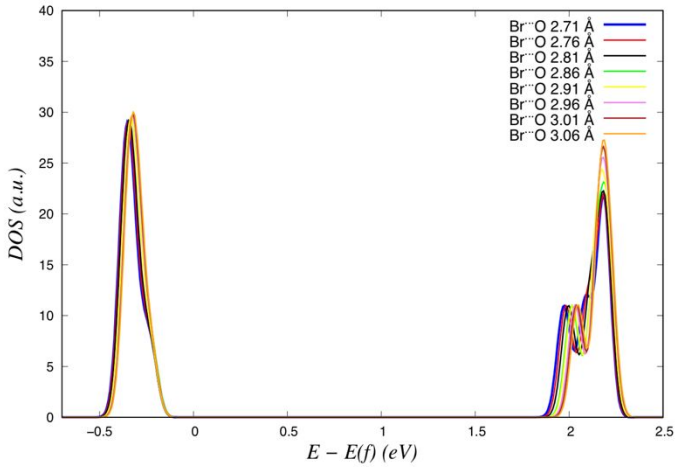

Figure 2 Total DOS of Br6A Crystal, with different *b* lattice constant. By decreasing *b* lattice constant, the halogen bond length decreases accordingly and there is a red shift in the LUMO states. All spectra are aligned relative to the Fermi level.

The second-order E(2) interaction energies we calculated are reported in table 2. This analysis is carried out by examining all possible interactions between filled Lewis-type NBOs and empty non-Lewis NBOs, estimating their energetic importance via 2nd-order perturbation theory. The strongest interaction is identified for the interaction of the lone-pair orbitals of oxygen with the adjacent sigma* C-X (X=F, Cl, Br, and I) bonds of the neighboring molecule. As expected, bromine and iodine form the strongest halogen bonds with second-order E(2) interaction energies of 4.39 and 10.12 kcal/mol, respectively.

The excited-state properties and the nature of the singlet and triplet states of X6A molecules have been examined using TD-DFT calculations. All the X6A molecules exhibit (nπ*) S_1 and (ππ*) T_3 states. After excitation to the (nπ*) S_1 state it undergoes efficient intersystem crossing to the triplet manifold. The presence of oxygen atom in the aldehyde group generates the nπ* state and leads to strong spin–orbit coupling (SOC) that facilitates intersystem crossing from (nπ*) S_1 to (ππ*) T_3 according to El-Sayed's rule,[39,40] followed by internal conversion to the (ππ*) T_1 state.

As mentioned earlier, the relaxation of the Br6A crystal yields a lattice constant of b = 9.636 Å, and a halogen bond length of 2.807 Å. The b lattice constant, as well as the halogen bond length are deliberately increased to investigate the effect of halogen bonding on the density of states (DOS) and the HOMO-LUMO energy gap. As can be seen in Fig. 2, which shows the DOS near the HOMO-LUMO gap, decreasing the halogen bond length results in a red shift of the LUMO states. We surmise that HOMO and LUMO orbitals include mostly oxygen and bromine interactions, which cause the change in the energy gap. A more precise analysis is provided below. F6A, Cl6A and I6A also exhibit the same trend as Br6A, where I6A exhibits the greatest decrease in the LUMO energies, since it has the strongest halogen bonding interaction.

The projected DOS plot in Fig. 3 and HOMO-LUMO orbital

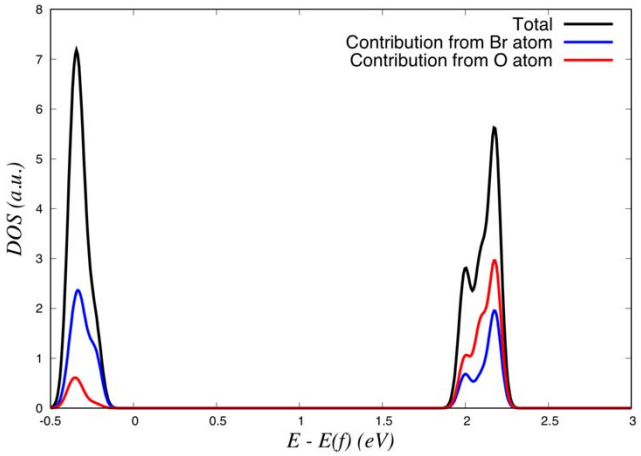

Figure 3 Site projected electronic density of states of Crystal Br6A. Bromine in crystal (blue trace), oxygen in crystal (red trace), total density of states of Br6A crystal (black trace). All spectra are aligned relative to the Fermi level.

renders in Fig. 4 also reveal the contribution of the Br and O in HOMO and LUMO states. It is known that aromatic aldehydes produce triplet states with high quantum yield at room temperature.[41, 42] It is expected that HOMO and LUMO states of Br6A molecule localize on the benzaldehyde group, but as can be seen in Fig. 4, the bromine atom also contributes to the HOMO and LUMO states. Such a contribution may be uniquely useful. The configuration of the oxygen of the aromatic carbonyl group adjacent to a bromine exhibits some degree of spin–orbit coupling. However, because of the heavy atom effect, bromine shows stronger spin–orbit coupling

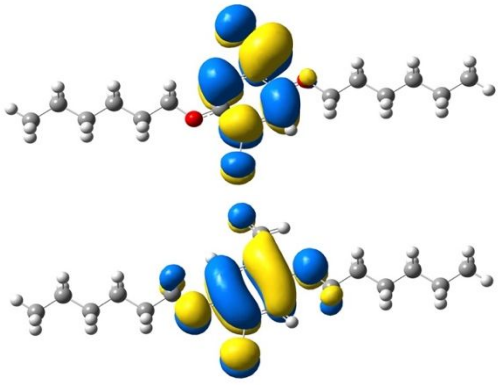

Figure 4 Calculated distributions of HOMO (bottom) and LUMO (top) orbitals of the Br6A molecule using B3LYP/6-31g(d,p) level in vacuum

interactions. In Br6A molecules, carbonyl oxygen internally, and bromine of the neighboring molecule externally promote singlet-triplet conversion and improve the phosphorescence property of these molecules.

Among the interesting advantages of the triplet–producing aromatic aldehydes is the possibility of generating triplet states from other molecules by direct transfer of energy from carbonyl triplets to a neighboring molecule.[41, 43] As mentioned

earlier, the quantum yield of Br6A is enhanced by diluting Br6A into the crystals of Br6. We hypothesize that triplet states produced by Br6A molecules transfer to Br6 molecules and the presence of two bromines in the Br6 molecule increases the spin–orbit coupling interactions, which, in turn, promotes the phosphorescence emission.

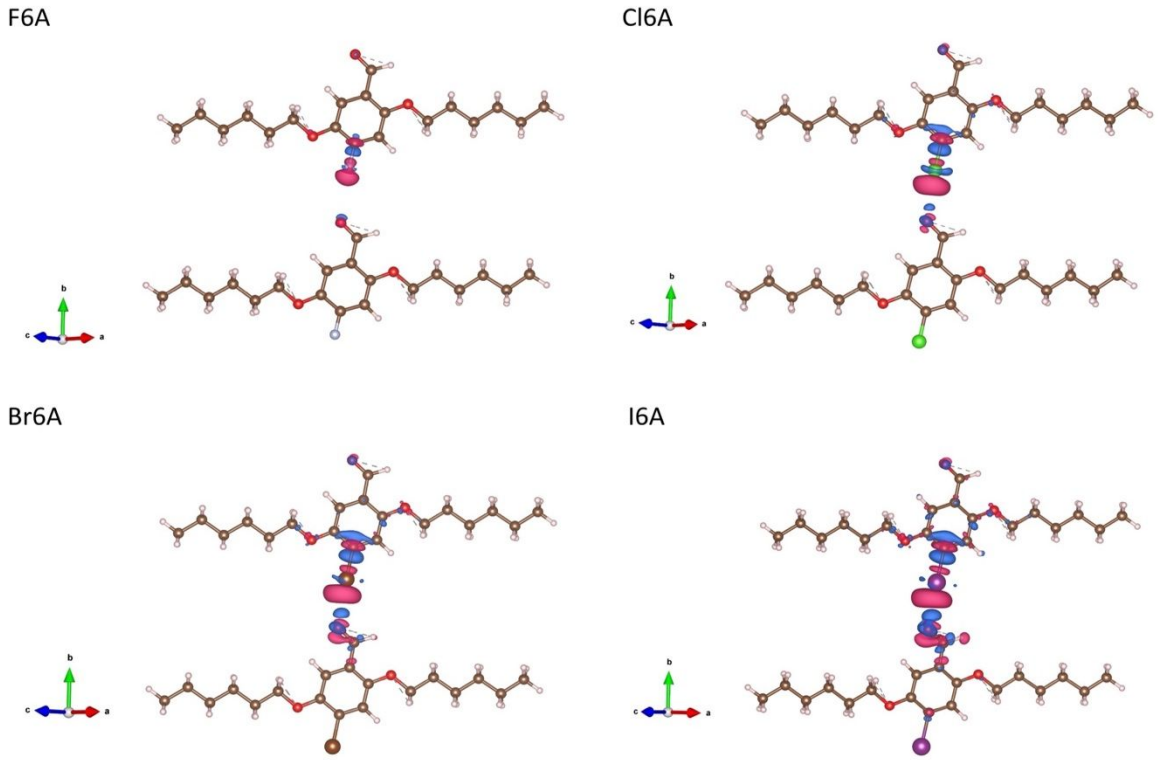

Figure 5 Charge density difference plots of X6A with the isosurface level of 0.0006 eÅ^{-3}. Blue and red regions denote loss (depletion) and gain (accumulation) of charges, respectively. *a* lattice constant is along x axis, *b* lattice constant is along y axis, and *c* lattice constant is along z axis.

To illustrate the detailed nature of the X-O (X=F, Cl, Br, and I) halogen bonding, we illustrate the charge redistribution by means of the electron density difference. The electron density difference, $\Delta\rho$, directly reveals where and how much the electron gain and loss take place, and is defined as

$$\Delta\rho = \rho_{dimer} - (\rho_{X6A_1} + \rho_{X6A_2}),$$

where ρ_{dimer} is the electron density of the combined two molecules of X6A (dimer), while ρ_{X6A_1} and ρ_{X6A_2} are the electron densities of the isolated individual molecules, which are calculated by freezing the atomic positions of the respective dimer system. It should be noted that $\Delta\rho$ is a function of the x-, y-, and z-coordinates, and therefore, it is impossible to give a quantitative three-dimensional representation of it in a single figure. Instead, Fig. 5 shows the charge density difference plots of X6A with the isosurface level of 0.0006 eÅ^{-3}, where the density differences can be qualitatively assessed. Blue and red regions denote loss (depletion) and gain (accumulation) of charges, respectively.

As in many other works,[44–46] we chose to calculate the plane-averaged electron density difference (PAEDD) along the direction of the halogen bonding, which allows for a quantitative evaluation of electron redistribution upon formation of the halogen bonds. PAEDD is the average of electron density difference ($\Delta\rho$) on a certain plane, which in this work is defined as

$$\sigma(y) = \frac{1}{A}\iint_A \Delta\rho(r)dxdz,$$

where $\Delta\rho(r)$ is the electron density difference at point r and A is the area of x-z-plane, perpendicular to the hydrogen bonding direction (y-direction).

Fig. 6 shows the plane-averaged electron density difference (PAEDD) along the direction of the halogen bonding, which allows for a quantitative evaluation of electron redistribution upon formation of these halogen bonds. This figure reveals the nature of halogen bonding between the halogen X (X=F, Cl, Br, and I) and the oxygen of the nearest molecule. Solid lines represent a charge accumulation region and dotted lines represent charge depletion regions.

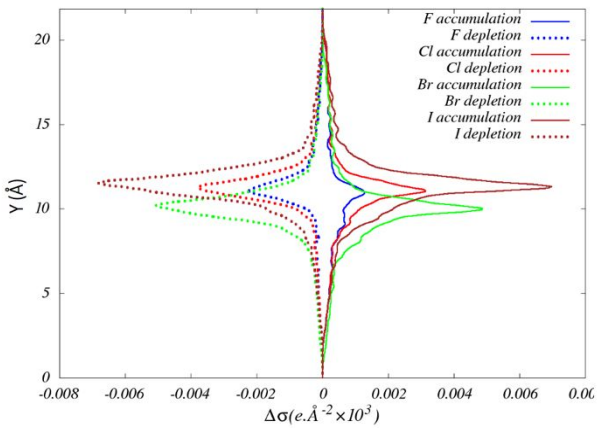

Figure 6 Plot of the plane-averaged electron density difference along the direction of the halogen bonding. The solid and dotted line represent charge accumulation and depletion, respectively.

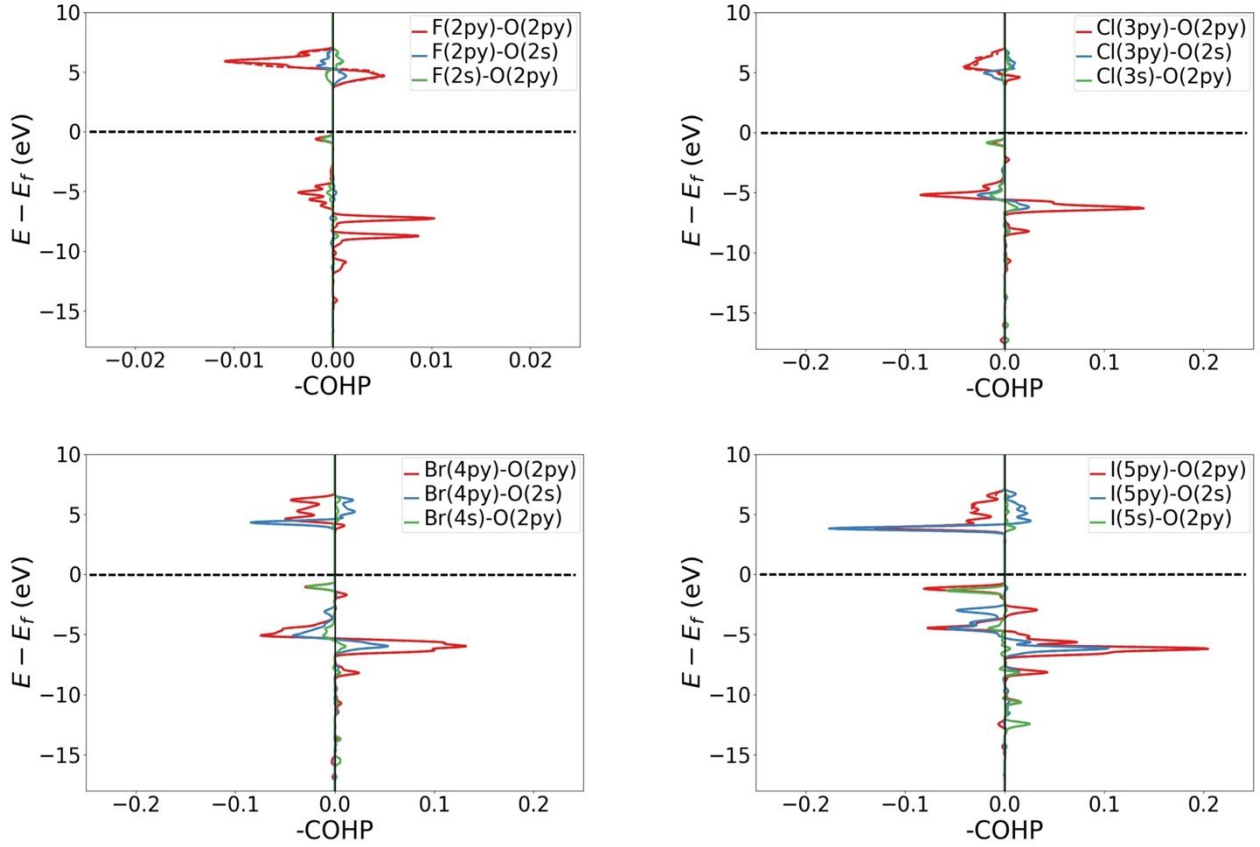

Figure 7 COHP analysis for halogen and Oxygen orbitals. The various components show the dominating orbital interactions in each case. Note that x axis for F is ten times smaller than others. All spectra are aligned relative to the Fermi level.

Accumulation of more charge along the X-O (X=F, Cl, Br, and I) signifies an enhancement of halogen bonding. Evaluation of the integrals of $\Delta\sigma$ suggested that the charge accumulation for the X6As are as follows: F 0.0653 e, Cl 0.103 e, Br 0.139 e, I 0.195 e. As expected, I6A exhibits the most accumulation of charge, which is consistent with it forming the strongest halogen bond, while F6A incurs the least accumulation of charge.

The above discussion of charge redistribution into hybrid states is a global view of overall orbital types and energies. The nature of the halogen bonds can be understood by considering the crystal orbital Hamilton populations (COHP) analysis.[47, 48] The DOS analysis shows where the electrons are, but nothing about their bonding character. However, a COHP diagram shows the bonding (positive values) and antibonding (negative values) contributions to the band-structure energy. It divides the band-structure energy into orbital-pair interactions; in other words, it is a bond-weighted DOS between a pair of adjacent atoms. Fig. 7 shows the COHP analyses, obtained with the LOBSTER (Local Orbital Basis Suite Towards Electronic-Structure Reconstruction) code.[49] These are normalized by the number of bonds and are represented with reversed sign, so that positive values of the COHP represent bonding, and negative values antibonding contributions.

We carried out COHP analyses for different combinations of *s*, p_x, p_y, and p_z orbitals between halogen and the oxygen of the neighboring molecule for X6A (X=F, Cl, br, I). Since the halogen bonding is in y-direction, we find that only *s* and p_y orbitals have large COHP peaks. Therefore, here, we have only presented the COHP diagrams of the s and p_y orbitals. In Fig. 7, for F6A, we notice strong bonding contributions from F2p_y-O2p_y in the interval from –11 eV to -7 eV, but also some antibonding contributions in the intervals from –6 eV to -4 eV and from –1 eV to 0 eV. However, COHP strength is significantly reduced compared to the other halogens, which also indicates weak halogen bonding strength in F6A case.

On the other hand, we observe substantial bonding contributions from X-O (X=Cl, Br, and I) in the interval from -9 eV to -1 eV, accompanied by smaller antibonding contributions in the interval from -5 eV to -1 eV. The larger footprint of X-O bonding contributions noticed in the COHP for I-O in comparison to X-Br(Cl), compounded with the bonding charge density of X-O bonds described earlier, suggests that the bonding contributions increase from Cl, Br, and I, respectively.

4 Conclusions

We report a first-principles quantum mechanical investigation of Br6A and its derivatives based on DFT and TD-

DFT methods, in order to explain experimentally observed properties and to provide guidance for the design of purely organic phosphorescence compounds. The presence of halogen bonding in Br6A and other derivatives of this molecule are demonstrated. It is revealed that iodine forms the strongest halogen bonding interaction and fluorine forms the weakest interaction. The strong halogen bonding present in crystals of Br6A and I6A more effectively suppress vibrations and prevent non–radiative decays compared to F and Cl derivatives. Along with suppression of vibration-induced losses, for heavy atoms, spin-orbit coupling is large and a change in spin is thus more favorable. Consequently, triplet to singlet transitions are most common in molecules containing iodine and bromine. This work also highlights that there is a decrease in electrical energy band gap as larger halogens are involved. The dependence of energy band gap on the halogen species is important in the context of tuning molecules for their emission colors. For device fabrication, film forming materials, like polymers and amorphous solids are preferred. Although these molecules are very promising for developing purely organic phosphors, they still cannot be used for practical applications because they require crystalline materials. However, the insights gained from computational analyses can serve to develop materials design strategies for suppressing vibrational losses in polymers and amorphous solids.

Conflicts of interest

There are no conflicts to declare.

Acknowledgements

This research was supported by funding from the US National Science Foundation, grant number **NSF DMR-1435965**.

References

1 O. Bolton, K. Lee, H.-J. Kim, K. Y. Lin and J. Kim, Activating efficient phosphorescence from purely organic materials by crystal design, *Nature chemistry*, 2011, **3**, 205-210.

2 C. W. Tang and S. A. VanSlyke, Organic electroluminescent diodes, *Applied physics letters*, 1987, **51**, 913-915.

3 C. Adachi, M. A. Baldo, M. E. Thompson and S. R. Forrest, Nearly 100% internal phosphorescence efficiency in an organic light-emitting device, *Journal of Applied Physics*, 2001, **90**, 5048-5051.

4 R. Ansari, W. Shao, S.-J. Yoon, J. Kim and J. Kieffer, Charge Transfer as the Key Parameter Affecting the Color Purity of Thermally Activated Delayed Fluorescence Emitters, *ACS Applied Materials & Interfaces*, 2021, **13**, 28529-28537.

5 S. Kappaun, C. Slugovc and E. J. List, Phosphorescent organic light-emitting devices: working principle and iridium based emitter materials., *Int J Mol Sci*, 2008, **9**, 1527-1547.

6 M. Kim, S. Yoon, S. H. Han, R. Ansari, J. Kieffer, J. Y. Lee and J. Kim, Molecular Design Approach Managing Molecular Orbital Superposition for High Efficiency without Color Shift in Thermally Activated Delayed Fluorescent Organic Light-Emitting Diodes, *Chemistry–A European Journal*, 2019, **25**, 1829-1834.

7 G. Zhou, W. Wong and X. Yang, New Design Tactics in OLEDs Using Functionalized 2-Phenylpyridine-Type Cyclometalates of Iridium (III) and Platinum (II), *Chemistry–An Asian Journal*, 2011, **6**, 1706-1727.

8 M. A. Baldo, S. Lamansky, P. E. Burrows, M. E. Thompson and S. R. Forrest, Very high-efficiency green organic light-emitting devices based on electrophosphorescence, *Applied Physics Letters*, 1999, **75**, 4-6.

9 M. A. Baldo, D. F. O'Brien, Y. You, A. Shoustikov, S. Sibley, M. E. Thompson and S. R. Forrest, Highly efficient phosphorescent emission from organic electroluminescent devices, *Nature*, 1998, **395**, 151-154.

10 P. E. M. Siegbahn, Trends of metal-carbon bond strengths in transition metal complexes, *The Journal of Physical Chemistry*, 1995, **99**, 12723-12729.

11 Wang, S., Yuan, W. Z. and Zhang, Y. (2016) in Aggregation-Induced Emission: Materials and Applications Volume 2 Eds.), pp. 1-26, ACS Publications,

12 D. Lee, O. Bolton, B. C. Kim, J. H. Youk, S. Takayama and J. Kim, Room temperature phosphorescence of metal-free organic materials in amorphous polymer matrices, *Journal of the American Chemical Society*, 2013, **135**, 6325-6329.

13 M. S. Kwon, D. Lee, S. Seo, J. Jung and J. Kim, Tailoring intermolecular interactions for efficient room-temperature phosphorescence from purely organic materials in amorphous polymer matrices, *Angewandte Chemie*, 2014, **126**, 11359-11363.

14 G. Bergamini, A. Fermi, C. Botta, U. Giovanella, S. Di Motta, F. Negri, R. Peresutti, M. Gingras and P. Ceroni, A persulfurated benzene molecule exhibits outstanding phosphorescence in rigid environments: from computational study to organic nanocrystals and OLED applications, *Journal of Materials Chemistry C*, 2013, **1**, 2717-2724.

15 H. Y. Gao, Q. J. Shen, X. R. Zhao, X. Q. Yan, X. Pang and W. J. Jin, Phosphorescent co-crystal assembled by 1, 4-diiodotetrafluorobenzene with carbazole based on C–I··· π halogen bonding, *Journal of Materials Chemistry*, 2012, **22**, 5336-5343.

16 H. Y. Gao, X. R. Zhao, H. Wang, X. Pang and W. J. Jin, Phosphorescent cocrystals assembled by 1, 4-diiodotetrafluorobenzene and fluorene and its heterocyclic analogues based on C–I··· π halogen bonding, *Crystal growth & design*, 2012, **12**, 4377-4387.

17 Y. J. Gao, C. Li, R. Liu and W. J. Jin, Phosphorescence of several cocrystals assembled by diiodotetrafluorobenzene and three ring angular diazaphenanthrenes via CI··· N halogen bond, *Spectrochimica Acta Part A: Molecular and Biomolecular Spectroscopy*, 2017, **173**, 792-799.

18 S. Sarkar, H. P. Hendrickson, D. Lee, F. DeVine, J. Jung, E. Geva, J. Kim and B. D. Dunietz, Phosphorescence in bromobenzaldehyde can be enhanced through intramolecular heavy atom effect, *The Journal of Physical Chemistry C*, 2017, **121**, 3771-3777.

19 H. Saigusa and T. Azumi, Internal heavy atom effect on the triplet spin sublevels of the lowest triplet state of naphthalene. I. Radiative and nonradiative decays of the spin sublevels of 1-halonaphthalenes, *The Journal of Chemical Physics*, 1979, **71**, 1408-1413.

20 G. G. Giachino and D. R. Kearns, Nature of the external heavy-atom effect on radiative and nonradiative singlet–triplet transitions, *The Journal of Chemical Physics*, 1970, **52**, 2964-2974.
21 S. P. McGlynn, R. Sunseri and N. Christodouleas, External Heavy-Atom Spin-Orbital Coupling Effect. I. The Nature of the Interaction, *The Journal of Chemical Physics*, 1962, **37**, 1818-1824.
22 P. G. Seybold and W. White, Room temperature phosphorescence analysis. Use of the external heavy-atom effect, *Analytical Chemistry*, 1975, **47**, 1199-1200.
23 Glossary of Terms Used in Photochemistry, 3rd Edition (IUPAC Recommendations 2006), 2007, 331.
24 D. W. Oxtoby, H. P. Gillis and N. H. Nachtrieb, Principles of Modern Chemistry, 1999,
25 G. Kresse and J. Hafner, Ab initio molecular-dynamics simulation of the liquid-metal–amorphous-semiconductor transition in germanium, *Physical Review B*, 1994, **49**, 14251.
26 G. Kresse and J. Furthmüller, Efficiency of ab-initio total energy calculations for metals and semiconductors using a plane-wave basis set, *Computational materials science*, 1996, **6**, 15-50.
27 J. P. Perdew, K. Burke and M. Ernzerhof, Generalized gradient approximation made simple, *Physical review letters*, 1996, **77**, 3865.
28 P. E. Blöchl, Projector augmented-wave method, *Physical review B*, 1994, **50**, 17953.
29 G. Kresse and D. Joubert, From ultrasoft pseudopotentials to the projector augmented-wave method, *Physical review b*, 1999, **59**, 1758.
30 H. J. Monkhorst and J. D. Pack, Special points for Brillouin-zone integrations, *Physical review B*, 1976, **13**, 5188.
31 A. Tkatchenko, R. A. DiStasio Jr, R. Car and M. Scheffler, Accurate and efficient method for many-body van der Waals interactions, *Physical review letters*, 2012, **108**, 236402.
32 S. Steiner, S. Khmelevskyi, M. Marsmann and G. Kresse, Calculation of the magnetic anisotropy with projected-augmented-wave methodology and the case study of disordered Fe 1− x Co x alloys, *Physical Review B*, 2016, **93**, 224425.
33 M. J. Frisch, G. W. Trucks, H. B. Schlegel, G. E. Scuseria, M. A. Robb, J. R. Cheeseman, G. Scalmani, V. Barone, G. A. Petersson, H. Nakatsuji, X. Li, M. Caricato, A. V. Marenich, J. Bloino, B. G. Janesko, R. Gomperts, B. Mennucci, H. P. Hratchian, J. V. Ortiz, A. F. Izmaylov, J. L. Sonnenberg, Williams, F. Ding, F. Lipparini, F. Egidi, J. Goings, B. Peng, A. Petrone, T. Henderson, D. Ranasinghe, V. G. Zakrzewski, J. Gao, N. Rega, G. Zheng, W. Liang, M. Hada, M. Ehara, K. Toyota, R. Fukuda, J. Hasegawa, M. Ishida, T. Nakajima, Y. Honda, O. Kitao, H. Nakai, T. Vreven, K. Throssell, J. A. Montgomery Jr., J. E. Peralta, F. Ogliaro, M. J. Bearpark, J. J. Heyd, E. N. Brothers, K. N. Kudin, V. N. Staroverov, T. A. Keith, R. Kobayashi, J. Normand, K. Raghavachari, A. P. Rendell, J. C. Burant, S. S. Iyengar, J. Tomasi, M. Cossi, J. M. Millam, M. Klene, C. Adamo, R. Cammi, J. W. Ochterski, R. L. Martin, K. Morokuma, O. Farkas, J. B. Foresman and D. J. Fox, Gaussian 16 Rev. C.01, 2016,
34 P. Metrangolo and G. Resnati, Halogen Bonding: A Paradigm in Supramolecular Chemistry, *Chem. Eur. J.*, 2001, **7**, 2511-2519.
35 G. R. Desiraju, P. S. Ho, L. Kloo, A. C. Legon, R. Marquardt, P. Metrangolo, P. Politzer, G. Resnati and K. Rissanen, Definition of the halogen bond (IUPAC Recommendations 2013), *Pure Appl. Chem*, 2013, **85**, 1711-1713.
36 P. Politzer, P. Lane, M. C. Concha, Y. Ma and J. S. Murray, An overview of halogen bonding, *Journal of molecular modeling*, 2007, **13**, 305-311.
37 P. Metrangolo, H. Neukirch, T. Pilati and G. Resnati, Halogen bonding based recognition processes: a world parallel to hydrogen bonding, *Accounts of chemical research*, 2005, **38**, 386-395.
38 T. Clark, M. Hennemann, J. S. Murray and P. Politzer, Halogen bonding: the σ-hole, *Journal of molecular modeling*, 2007, **13**, 291-296.
39 M. Baba, Intersystem Crossing in the 1nπ* and 1ππ* States, *The Journal of Physical Chemistry A*, 2011, **115**, 9514-9519.
40 K. Bhattacharyya and A. Datta, Visible-Light-Mediated Excited State Relaxation in Semi-Synthetic Genetic Alphabet: d5SICS and dNaM, *Chemistry–A European Journal*, 2017, **23**, 11494-11498.
41 H. L. J. Bäckström and K. Sandros, Transfer of Triplet State Energy in Fluid Solutions, *Acta Chemica Scandinavica*, 1960, **14**, 48-62.
42 G. S. Hammond and W. M. Moore, The role of a triplet state in the photoreduction of benzophenone, *Journal of the American Chemical Society*, 1959, **81**, 6334-6334.
43 G. O. Schenck and R. Steinmetz, Neuartige durch Benzophenon photosensibilisierte Additionen von Maleinsäureanhydrid an Benzol und andere Aromaten, *Tetrahedron Letters*, 1960, **1**, 1-8.
44 B. Meyer and D. Vanderbilt, Ab initio study of BaTiO 3 and PbTiO 3 surfaces in external electric fields, *Physical Review B*, 2001, **63**, 205426.
45 Y. B. Xue, Y. Y. Shan and H. Xu, The role of boundary conditions in tuning the electronic properties of the (0 0 1) LaAlO3/SrTiO3 interface, *Computational Materials Science*, 2018, **149**, 354-359.
46 Y. Xue, C. Geng and Y. Guo, Two-Dimensional (001) LaAlO3/SrTiO3 Heterostructures with Adjustable Band Gap and Magnetic Properties, *ACS Applied Materials & Interfaces*, 2019, **12**, 3134-3139.
47 V. L. Deringer, A. L. Tchougréeff and R. Dronskowski, Crystal orbital Hamilton population (COHP) analysis as projected from plane-wave basis sets, *The journal of physical chemistry A*, 2011, **115**, 5461-5466.
48 R. Dronskowski and P. E. Blöchl, Crystal orbital Hamilton populations (COHP): energy-resolved visualization of chemical bonding in solids based on density-functional calculations, *The Journal of Physical Chemistry*, 1993, **97**, 8617-8624.
49 S. Maintz, V. L. Deringer, A. L. Tchougréeff and R. Dronskowski, LOBSTER: A tool to extract chemical bonding from plane-wave based DFT, *Journal of computational chemistry*, 2016, **37**, 1030-1035.